

Computational Design of Epitope-Scaffolds Allows Induction of Antibodies Specific for a Poorly Immunogenic HIV Vaccine Epitope

Bruno E. Correia,^{1,2,6} Yih-En Andrew Ban,^{1,6,7} Margaret A. Holmes,³ Hengyu Xu,³ Katharine Ellingson,⁴ Zane Kraft,⁴ Chris Carrico,¹ Erica Boni,³ D. Noah Sather,⁴ Camille Zenobia,³ Katherine Y. Burke,³ Tyler Bradley-Hewitt,³ Jessica F. Bruhn-Johannsen,³ Oleksandr Kalyuzhnyi,¹ David Baker,¹ Roland K. Strong,³ Leonidas Stamatatos,^{4,5} and William R. Schief^{1,*}

¹Department of Biochemistry, University of Washington, Seattle, WA 98195, USA

²Instituto de Tecnologia Química e Biológica, Universidade Nova de Lisboa, Oeiras 2780-157, Portugal

³Division of Basic Sciences, Fred Hutchinson Cancer Research Center, Seattle, WA 98109-1024, USA

⁴Seattle Biomedical Research Institute, Seattle, WA 98109-5219, USA

⁵Department of Global Health, University of Washington, Seattle, WA 98195, USA

⁶These authors contributed equally to this work

⁷Present address: Arzeda Corporation, Seattle, WA 98102, USA

*Correspondence: schief@u.washington.edu

DOI 10.1016/j.str.2010.06.010

SUMMARY

Broadly cross-reactive monoclonal antibodies define epitopes for vaccine development against HIV and other highly mutable viruses. Crystal structures are available for several such antibody-epitope complexes, but methods are needed to translate that structural information into immunogens that re- elicit similar antibodies. We describe a general computational method to design epitope-scaffolds in which contiguous structural epitopes are transplanted to scaffold proteins for conformational stabilization and immune presentation. Epitope-scaffolds designed for the poorly immunogenic but conserved HIV epitope 4E10 exhibited high epitope structural mimicry, bound with higher affinities to monoclonal antibody (mAb) 4E10 than the cognate peptide, and inhibited HIV neutralization by HIV+ sera. Rabbit immunization with an epitope-scaffold induced antibodies with structural specificity highly similar to mAb 4E10, an important advance toward elicitation of neutralizing activity. The results demonstrate that computationally designed epitope-scaffolds are valuable as structure-specific serological reagents and as immunogens to elicit antibodies with predetermined structural specificity.

INTRODUCTION

A protective HIV vaccine, or a universal flu vaccine, likely will elicit antibodies that block infection of diverse circulating strains of HIV or influenza. Several anti-HIV antibodies with broad neutralizing reactivities have been isolated from natural infection, and approximately 25% of HIV-1-infected individuals produce broadly neutralizing sera (for review, see [Stamatatos et al.](#),

2009), but efforts to elicit such responses by vaccination have failed. Anti-influenza broadly neutralizing antibodies (bNAbs) also have been characterized ([Kashyap et al.](#), 2008; [Okuno et al.](#), 1993; [Sui et al.](#), 2009; [Throsby et al.](#), 2008), but the annual influenza vaccine elicits potent neutralizing antibodies only against the vaccine strains and closely related isolates.

The anti-HIV mAb 4E10 neutralizes 98% of HIV strains ([Binley et al.](#), 2004); hence, elicitation of 4E10-like antibodies is a major goal for HIV vaccine design. 4E10 binds a contiguous epitope in the membrane proximal external region (MPER) of gp41 just N-terminal to the transmembrane domain ([Stiegler et al.](#), 2001; [Zwick et al.](#), 2001), an epitope that is likely only transiently exposed during viral fusion with the target cell ([Frey et al.](#), 2008). Nuclear magnetic resonance structural analysis of MPER peptides in lipid micelles found a kinked helix partially embedded in lipid ([Sun et al.](#), 2008). Crystal structures of mAb 4E10 in complex with gp41 peptides revealed that 4E10 binds to a helical epitope in an end-on manner with the N terminus and one face of the helix docked into a hydrophobic cavity on the antibody; the bound epitope adopts a short 3/10 helix followed by an alpha helix, and conserved HIV side chains from both regions make significant antibody contacts ([Cardoso et al.](#), 2005, 2007; [Scherer et al.](#), 2010; [Xu et al.](#), 2009). The antibody also has a long, hydrophobic complementarity-determining region H3 (CDR H3) loop, which does not bind directly to the helical epitope but which may provide contacts to the viral lipid membrane and contribute to neutralization ([Cardoso et al.](#), 2005, 2007; [Scherer et al.](#), 2010; [Xu et al.](#), 2009). Here, as a first step to elicit antibodies with the binding and neutralizing properties of mAb 4E10, we aimed to develop immunogens that would elicit antibodies with the exact binding specificity of mAb 4E10 for its core peptide epitope.

A major hurdle confronting 4E10-vaccine design is that the epitope is naturally poorly immunogenic. While 4E10-like activity has been detected in HIV+ patients with broadly neutralizing activity, the frequency is low (~5%) ([Binley et al.](#), 2008; [Li et al.](#), 2009; [Sather et al.](#), 2009). Furthermore, previous attempts to elicit 4E10-like antibodies by vaccination using soluble

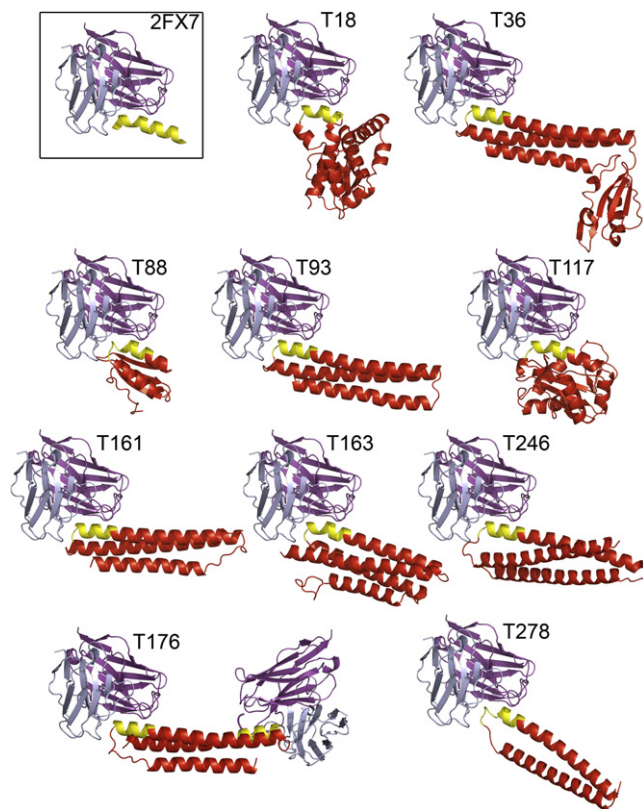


Figure 1. Models of 4E10 Fv/Epitope-Scaffold Complexes

The helical 4E10 epitope (yellow) was transplanted from the 4E10 Fab/gp41 peptide complex (boxed at top left) onto different scaffold proteins (red).

trimeric gp140 (Derby et al., 2006), VLP-membrane-anchored gp41 variants (Kim et al., 2007), or a gp120 construct with the 4E10 epitope embedded in the highly immunogenic V2 loop (Law et al., 2007), failed to elicit reactivity against the epitope primary sequence. MPER peptides anchored to liposomes or hepatitis B surface antigen particles have elicited modest responses against 4E10 peptides (Phogat et al., 2008; Watson and Szoka, 2009), but whether these responses were directed to the 4E10 epitope or other epitopes was not determined. In none of these cases was the helical epitope conformation necessarily stabilized, though in all cases the antigens did bind to mAb 4E10.

Crystallographic analysis of several anti-HIV (Calarese et al., 2003; Cardoso et al., 2005; Ofek et al., 2004; Zhou et al., 2007) and anti-influenza (Ekiert et al., 2009; Sui et al., 2009) bNAbs/epitope complexes, combined with advances in computational protein design (Kuhlman et al., 2003), provides new opportunities for structure-based vaccine design (Dormitzer et al., 2008). Here, we pursued a strategy of stabilizing an epitope in its antibody-bound conformation, and presenting that stabilized epitope in an immunogenic format, in order to elicit antibodies with structural specificity similar to the target antibody. Specifically, we engineered “epitope-scaffold” immunogens in which the HIV 4E10 epitope was transplanted by computational design to small, nonviral scaffold proteins for conformational stabilization and presentation to the immune system without the immu-

nodominant variable regions typical of persistent pathogens. The computational design methods are general and should be applicable for structural stabilization of a variety of contiguous epitopes of different conformations from HIV, influenza, and other viruses.

RESULTS

Computational Design of Epitope-Scaffolds

We designed a total of 103 4E10 epitope-scaffolds by the side-chain grafting method (models representative of the variety of scaffold topologies are shown in Figure 1). This method entailed “matching” and “design” stages. In the automated “matching” stage, a subset of the Protein Data Bank (PDB) (Berman et al., 2000) was exhaustively searched for scaffold proteins with a surface-exposed backbone segment similar in conformation to the 4E10 epitope (NWFDITxxLW in PDB ID: 2FX7; Cardoso et al., 2007). The resulting “hits” were filtered first by backbone clash with the antibody and second by antibody-epitope binding energy (epitope side chains were transferred to the scaffold and energy minimization (Gray et al., 2003) was used to optimize antibody and epitope side-chain conformations as well as the antibody-scaffold rigid-body orientation). Scaffolds selected in the “matching” stage were taken to the semiautomated design stage in which amino acids were designed for scaffold positions outside the epitope. The design stage aimed to ensure scaffold stability and solubility, avoid additional interactions between scaffold and antibody, support the optimized epitope side-chain conformations, eliminate undesired functional sites, and trim extraneous domains.

“Validated” Epitope-Scaffolds Are Stable and Bind mAb 4E10 with High Affinity

Epitope-scaffolds were expressed in *Escherichia coli*, purified by immobilized metal affinity chromatography and size-exclusion chromatography (SEC), and screened for 4E10 Fv binding in qualitative SEC assays. Constructs were validated if they expressed as soluble protein (not within inclusion bodies) and were purifiable to stable, soluble species that bound Fv by SEC; nonvalidated constructs were eliminated from further consideration. A total of 135 constructs were tested for expression (103 designs plus 32 purification tag variants), and, of those, 24 different designs (23% of 103 designs) were carried forward for quantitative analysis of mAb-binding by surface plasmon resonance (SPR). Biophysical data are collected in Table 1 for the representative set of 10 validated 4E10 epitope-scaffolds depicted in Figure 1, and background information on each scaffold is provided in Table S1 (available online).

To facilitate interpretation of mAb 4E10-binding experiments, the epitope-scaffold solution multimer state and stoichiometry of Fv-binding were assessed by static light scattering (SLS) and SEC. Examples of SEC data are given in Figure S1. Solution multimer state and Fv-binding stoichiometry accorded with expectation (monomer and 1:1, or dimer and 2:2 for T18) for 5 of 12 epitope-scaffolds (T18, T36, T93, T161, T278). The other epitope-scaffolds formed unexpected multimers that dissociated in the presence of Fv, suggesting that multimers self-associating through the hydrophobic 4E10 epitope were in equilibrium with rare monomers. Aggregation was noted

Table 1. Solution Properties of 4E10 Epitope-Scaffolds

Epitope-Scaffold	Solution Multimer State	T _m (°C)	Fv:Epitope-Scaffold Binding Stoichiometry	Interaction Parameters (SPR)					
				Analyte: 4E10 Fv Ligand: Epitope-Scaffold ^a			Analyte: Epitope-Scaffold Ligand: 4E10 IgG ^b		
				k _{OFF} /k _{ON} (nM)	k _{ON} (M ⁻¹ s ⁻¹)	k _{OFF} (s ⁻¹)	k _{OFF} /k _{ON} (nM)	k _{ON} (M ⁻¹ s ⁻¹)	k _{OFF} (s ⁻¹)
T18	Dimer	≥ 100	2:2	Low Specific Activity ^c	Low Specific Activity ^c	Low Specific Activity ^c	2.75	1.47 × 10 ⁵	4.05 × 10 ⁻⁴
T36	Monomer	44	1:1	0.014	5.89 × 10 ⁶	8.34 × 10 ⁻⁵	0.044	1.95 × 10 ⁶	8.59 × 10 ⁻⁵
T88	Tetramer	64	2:2	5.6	1:4.0 × 10 ⁵ 2:2.24 × 10 ⁻²	1:4.8 × 10 ⁻² 2:1.1 × 10 ⁻³	0.047	3.94 × 10 ⁶	1.87 × 10 ⁻⁴
T93	Monomer	79	1:1	0.0075	6.98 × 10 ⁶	5.23 × 10 ⁻⁵	0.028	3.17 × 10 ⁶	8.73 × 10 ⁻⁵
T117	Dimer	56	1:1	Low Specific Activity ^c	Low Specific Activity ^c	Low Specific Activity ^c	≤ 0.01 ^d	–	–
T161	Monomer	65	1:1	0.015	7.92 × 10 ⁶	1.15 × 10 ⁻⁴	0.11	3.10 × 10 ⁶	3.43 × 10 ⁻⁴
T163	Monomer, dimer	72	Multiple species	0.263	2.57 × 10 ⁶	6.75 × 10 ⁻⁴	ND	ND	ND
T176	Monomer, dimer	48	Multiple species	0.14	4.49 × 10 ⁶	6.18 × 10 ⁻⁴	0.051	6.44 × 10 ⁶	3.26 × 10 ⁻⁴
T246	Monomer, dimer, trimer	62	1:1	3.3	1:2.34 × 10 ⁶ 2:3.06 × 10 ⁻³	1:1.66 × 10 ⁻² 2:2.62 × 10 ⁻³	ND	ND	ND
T278	Monomer	51	1:1	0.89	1:3.13 × 10 ⁶ 2:1.72 × 10 ⁻²	1:3.2 × 10 ⁻² 2:1.63 × 10 ⁻³	1.85	3.71 × 10 ⁵	6.84 × 10 ⁻⁴

Italicized values: SPR data were fit using a two-state interaction model; the second on-rate has units of sec⁻¹. ND: experiment not performed. For all reported values, standard error is ≤ ±3 of the last significant figure.

^a Epitope-scaffold was immobilized by direct amine-coupling on CM5 chip or by biotinylation and capture on SA chip.

^b 4E10 IgG was captured by amine-coupled anti-human IgG.

^c Coupling epitope-scaffold to chip results in an inactive surface, likely due to lysine residues neighboring the epitope.

^d Stated value is an upper limit on the K_D; off-rate was too slow to fit kinetics.

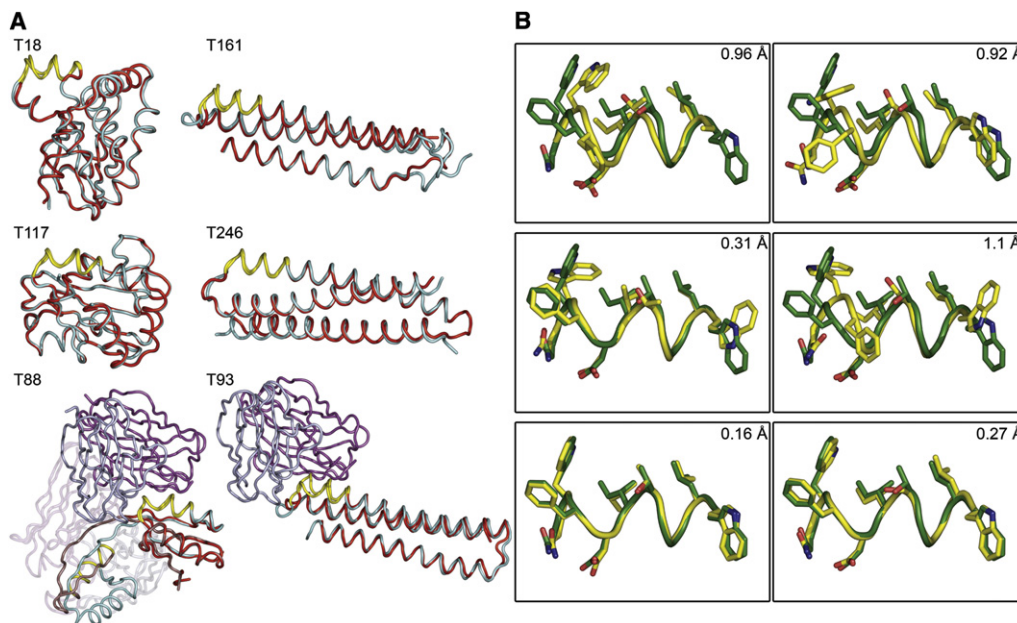


Figure 2. Crystallographic Analysis of 4E10 Epitope-Scaffolds

(A) Crystal structures of six epitope-scaffolds (cyan tubes) superimposed with design models (red tubes), with the epitope region colored yellow. Four structures are unliganded and two are complexed with 4E10 Fv W(H100A) (H-chain, light blue; L-chain, magenta). Resolution of structures was 2.3 (T18, PDB ID: 3LEF), 2.0 (T161, PDB ID: 3LF9), 1.9 (T117, PDB ID: 3LF6), 2.5 (T246, PDB ID: 3LG7), 2.65 (T88-Fv, PDB ID: 3LH2), and 2.8 (T93-Fv, PDB ID: 3LHP) Å.

(B) Epitope structure (yellow tubes and sticks) from each of the epitope-scaffold crystal structures, superimposed with the 4E10 Fab-bound structure of a gp41 peptide (green tube and sticks) from PDB ID 2FX7 (Cardoso et al., 2007). Backbone rmsd values between epitope-scaffold and peptide are indicated for each superposition.

previously for gp120 with engrafted MPER sequences (Law et al., 2007). Multimerization of some 4E10 epitope-scaffolds will be addressed in detail in a separate manuscript (H.X., M.C. Clifton, M.A.H., Della J. Friend, T. B.-H., J.F.B.-J., J. Burgner, L.S., and R.K.S., unpublished data).

Epitope-scaffold affinities for mAb 4E10 were generally quite high. Antibody binding affinity and kinetics were assessed by SPR in two formats: with 4E10 Fv in solution as “analyte” and epitope-scaffolds coupled to the sensor chip as “ligand” (to assess interactions without avidity), and with 4E10 IgG captured on the chip and epitope-scaffold in solution (to allow avidity). Examples of SPR data and fits are shown in Figure S2, and conditions for each SPR experiment are given in Table S2. With epitope-scaffolds on the chip, equilibrium dissociation constants (K_D) ranged from 8 pM to 6 nM, and all epitope-scaffolds bound 4E10 Fv more tightly than 4E10 peptides ($K_D = 10\text{--}20$ nM) (Brunel et al., 2006; Xu et al., 2009), gp41 ($K_D = 32\text{--}35$ nM) (Klein et al., 2009) or gp140 trimers from isolate SF162 ($K_D = 130$ nM) (Xu et al., 2009). The range of K_D s was similar with epitope-scaffolds as analytes (22 pM to 3 nM). Monomeric epitope-scaffolds exhibited similar K_D s in both formats, while 120-fold tighter binding due to bivalent avidity was detected for T88 ($K_D = 47$ pM versus 5.6 nM) and 2.7-fold tighter binding was detected for T176 ($K_D = 51$ pM versus 140 pM), consistent with stoichiometry data. In both formats, variations in both k_{on} and k_{off} contributed to variations in K_D .

Epitope-scaffolds showed a range of thermal stabilities assessed by circular dichroism temperature melt analysis ($T_m = 44^\circ\text{C}$ to $T_m \geq 100^\circ\text{C}$), though a majority (60%) were very

stable with $T_m > 60^\circ\text{C}$, and a large majority (80%) were stable with $T_m > 50^\circ\text{C}$.

Crystallographic Analyses Reveal High Epitope Structural Mimicry by 4E10 Epitope-Scaffolds

To assess epitope structural mimicry, crystal structures were determined for six different epitope-scaffolds, four of unliganded epitope-scaffolds, and two of complexes with a 4E10 Fv construct biochemically validated elsewhere (Xu et al., 2009) (Figure 2). Crystallization conditions are in Table S3; X-ray diffraction and refinement statistics are in Table 2; stereo images of electron density maps are given in Figure S3.

The overall conformations of the epitope-scaffolds agreed well with design models in five of six cases (Figure 2A), with backbone rmsd values between models and structures of 0.47, 0.50, 0.79, 1.14, and 1.26 Å for epitope-scaffolds T117, T18, T246, T93, and T161, respectively. The structure of the T88-Fv complex revealed an unintended domain-swapped dimer binding two Fv molecules, consistent with the 2:2 stoichiometry measured by SEC and SLS. Nevertheless both T88-Fv complexes were very similar to the design model; ignoring two residues that bridge the T88 dimer, backbone rmsd between the two Fv-monomer complexes and the model were 0.6 and 0.5 Å, respectively.

Most importantly, epitope mimicry was excellent in both Fv-bound and unbound epitope-scaffolds (Figure 2B). Backbone rmsd between epitope-scaffold and the 4E10-bound conformation of the gp41 peptide (Cardoso et al., 2007), computed over epitope residues 672–680, was 0.99, 0.31, 0.99, and 1.1 Å

Table 2. X-Ray Diffraction Data and Refinement Statistics for the Epitope-Scaffold Structures

	T18	T88-Fv	T93-Fv	T117	T161	T246
Data Collection						
Space group	P6 ₅ 22	P2 ₁	P2 ₁ 2 ₁ 2 ₁	P2 ₁ 2 ₁ 2 ₁	C222 ₁	P2 ₁ 2 ₁ 2 ₁
Cell dimensions	56.4, 56.4, 324.1 Å	75.9, 145.9, 78.6 Å; 92.5°	53.0, 88.6, 150.0 Å	49.2, 82.0, 94.2 Å	40.7, 75.4, 79.6 Å	91.6, 94.9, 108.4 Å
Resolution (Å) ^a	48.30–2.30 (2.38–2.30)	28.01–2.65 (2.74–2.65)	29.54–2.70 (2.80–2.70)	49.21–1.90 (1.97–1.90)	32.64–2.00 (2.07–2.00)	28.82–2.50 (2.59–2.50)
Number observed reflections ^a	115,705 (8910)	190,285 (17,961)	66,868 (4874)	133,236 (12,691)	38,309 (2008)	150,445 (12,033)
Number unique reflections ^a	13,770 (1304)	49,017 (4883)	19,356 (1705)	30,053 (2886)	8462 (755)	33,220 (3180)
Redundancy ^a	8.40 (6.83)	3.88 (3.68)	3.45 (2.86)	4.43 (4.40)	4.53 (2.66)	4.53 (3.78)
Completeness (%) ^a	93.7(91.5)	98.9 (98.6)	96.2 (85.5)	97.5 (95.2)	98.3 (89.9)	99.5 (96.8)
Rmerge ^a	0.086 (0.373)	0.095 (0.376)	0.102 (0.405)	0.057 (0.341)	0.052 (0.185)	0.107 (0.429)
Average I/σ (I) ^a	9.0 (3.9)	9.4 (2.7)	7.1 (2.2)	17.2 (2.6)	18.6 (4.0)	6.6 (2.0)
Structure Refinement						
Resolution (Å)	46.78–2.30	26.70–2.65	28.99–2.70	31.50–1.90	27.37–2.00	28.82–2.50
R _{work} /R _{free}	0.258/0.290	0.222/0.270	0.243/0.335	0.223/0.279	0.204/0.260	0.257/0.301
Number of atoms						
Protein	1275	9019	5112	2494	925	3155
Water	55	132	82	262	127	94
Other	4 (1 ethylene glycol)	—	4 (1 ethylene glycol)	15 (3 phosphates)	—	55 (11 sulfates)
Rmsd from ideal values						
Bond lengths (Å)	0.009	0.006	0.009	0.009	0.011	0.014
Bond angles (°)	1.146	0.927	1.132	1.056	1.004	1.189
Chiral volume (Å ³)	0.070	0.054	0.051	0.061	0.057	0.062
Ramachandran plot statistics						
Most favored regions (%)	95.8	90.4	90.0	94.1	100.0	99.4
Additional allowed regions (%)	3.5	9.2	9.6	5.9	0.0	0.6
Generously allowed regions (%)	0.0	0.0	0.0	0.0	0.0	0.0
Disallowed regions (%)	0.7 (1 res. ^b)	0.4 (4 res. ^c)	0.3 (2 res. ^c)	0.0	0.0	0.0
Estimated coordinate error (maximum likelihood e.s.u.) (Å)	0.19	0.240		0.17	0.137	0.208
Average B factor						
Protein	66.4	57.2	68.1	43.6	45.1	76.6
Water	58.6	49.7	49.6	49.7	50.9	73.7
Other	85.3		53.2	82.4		96.3

^a Values in parentheses correspond to the highest resolution shell.

^b Residue 129, which is in a γ -turn conformation, as is the 1.5 Å resolution parent structure 1Z6N.

^c Fv light chain residue 52 (51 by Kabat numbering) of all four chains, which is in a highly conserved γ -turn conformation.

for the unbound structures of T18, T117, T161, and T246 respectively, 0.16 Å for each monomer in the T88-Fv complex, and 0.31 Å in the T93-Fv complex. B-factor analysis indicated that the epitope backbones were generally as well ordered as the epitope-scaffolds overall (Figure S4). Side-chain mimicry was reduced in the unliganded structures (Figure 2B), but high affinities for Fv indicated that appropriate side-chain conformers were attainable. Indeed, intermolecular contacts within the unliganded crystals stabilized different epitope side-chain conformations at some positions (Figure S5). The T88-Fv and T93-Fv complexes demonstrated precise mimicry at the side-chain level, with all-atom epitope rmsd of 0.48 and 0.36 Å, respectively; these complexes reproduced nearly all atomic

contacts across the bNAb-peptide interface (Cardoso et al., 2005, 2007; Xu et al., 2009) but made some additional contacts (Tables S4–S6 and Figure S6).

Epitope-Scaffolds as Reagents Reveal That Neutralizing Activity in HIV+ Sera Has 4E10-Like Helical Specificity While Nonneutralizing Antipeptide Sera Does Not

Sather et al. (2009) recently found evidence for the presence of 4E10-like antibodies in the serum of one HIV+ individual (“VC10028”). Support for this finding came primarily from the fact that a 4E10 peptide, but not a scrambled 4E10 peptide, could inhibit a fraction of the neutralizing activity of this serum in an in vitro neutralization assay. There are many potential

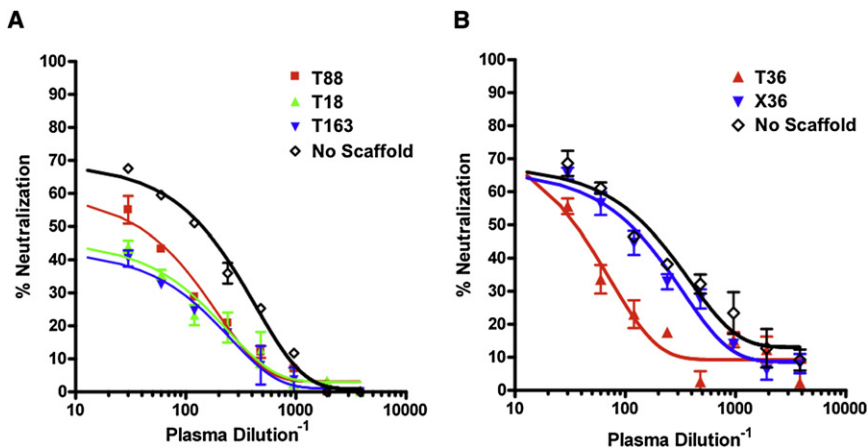


Figure 3. 4E10 Epitope-Scaffolds Inhibit Neutralizing Activity in HIV+ Serum VC10028

(A and B) Neutralization of JR-FL pseudovirus by serial dilutions of serum VC10028 (Sather et al., 2009) in the absence (open diamonds) or presence (solid shapes) of different 4E10 epitope-scaffolds at a concentration of 10 μ g/ml epitope-scaffolds. All epitope-scaffolds partially inhibit the neutralizing activity except a “dead-epitope” epitope-scaffold (X36, blue inverted triangles in B). Data are representative of three separate experiments; error bars represent means \pm SD.

antibody epitopes on the 4E10 peptide, especially given that the peptide likely samples many different conformations in solution, so the precise structural epitope(s) of the neutralizing antibodies in serum VC10028 could not be identified. Having demonstrated epitope structural mimicry crystallographically (Figure 2), we employed 4E10 epitope-scaffolds as reagents to determine whether the epitope conformation stabilized on the scaffolds was a target of the cross-neutralizing antibodies in VC10028. Several epitope-scaffolds inhibited the neutralizing activity of the sera (Figures 3A and 3B), but no inhibition was detected by a “dead-epitope” version of one scaffold (X36) in which the “WF” of the epitope was mutated to “ED” (Figure 3B). These results demonstrated that neutralizing antibodies targeting the helical epitope structure targeted by mAb 4E10 were present in the VC10028 sera. In contrast, nonneutralizing rabbit sera elicited by a 4E10 peptide-KLH conjugate had no significant affinity for any of several epitope-scaffolds tested, even though the peptide-KLH sera bound avidly to 4E10 peptide itself (Figure 4A). This result demonstrated that while the 4E10 peptide-KLH conjugate was immunogenic (one of three rabbits produced peptide-specific antibodies), it did not elicit antibodies with structural specificity similar to 4E10. Indeed, comparison of

4E10 binding is greatly diminished by mutants W672A, F673A, T676A, and L679A that remove critical contacts in the mAb/peptide crystal structure (Cardoso et al., 2005, 2007; Xu et al., 2009), but peptide-KLH sera binding to those mutants is undiminished. Together, these results showed how epitope-scaffolds may be useful as reagents to identify the presence or absence of precise structural specificities in sera and implied that epitope-scaffolds will be useful as “bait” to isolate antibodies targeting predefined structural epitopes.

An Epitope-Scaffold Elicited a Structurally Specific Antiepitope Response

The fact that the 4E10-like antibodies in serum VC10028 had structural specificity similar to mAb 4E10, while nonneutralizing antibodies in peptide-KLH sera did not, suggested that neutralization via the 4E10 epitope may require antibodies with 4E10-like structural specificity, and underscored the importance of testing epitope-scaffolds for their ability to re-elicite such structural specificity. To this end, we carried out immunization experiments with specific endotoxin-free preparations of one 4E10 epitope-scaffold (T88). Two groups of three rabbits were immunized with T88, one group with QS21 as adjuvant, and

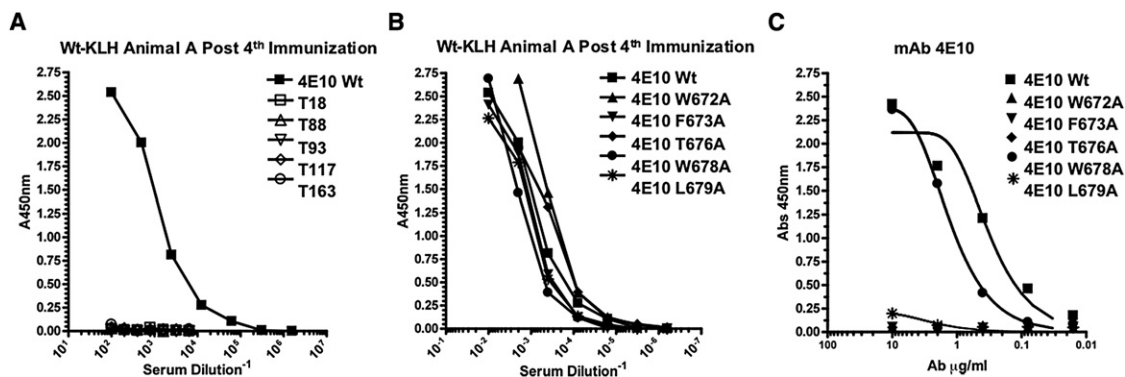


Figure 4. Structural Specificities of bNAb 4E10 and Anti-4E10 Peptide Rabbit Serum Are Dramatically Different

(A) ELISA of antipeptide serum binding to 4E10 peptide and different epitope-scaffolds. Data are the average of two experiments.

(B) ELISA of antipeptide serum binding to alanine mutant 4E10 peptides. Data are the average of three experiments.

(C) ELISA of bNAb 4E10 binding to alanine mutant 4E10 peptides. Data are the average of three experiments.

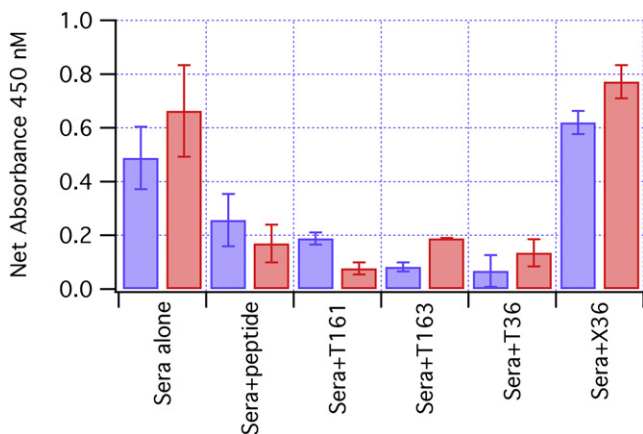


Figure 5. ELISA Binding of Anti-T88 Rabbit Sera to gp41 in Presence of Peptide and Epitope-Scaffold Competitors

Anti-T88 sera from two rabbits (blue, PEI adjuvant, five immunizations; red, QS21 adjuvant, six immunizations) binds to gp41 (“Sera alone”). Addition of peptide (“Sera+peptide”) or different scaffolds (“Sera+T161,” “Sera+T163,” “Sera+T36”) significantly reduces gp41 binding, but addition of a “dead-epitope” epitope-scaffold (“Sera+X36”) does not. ELISA response of prebleed rabbit sera to gp41 was subtracted from the data. Data were averaged from two or four experiments; error bars represent means \pm SD.

the other with PEI. One animal from each group developed antibodies that bound to HXB2 gp41, and this gp41-reactivity was inhibited by wild-type 4E10 peptide, demonstrating specific reactivity to the 4E10 epitope sequence (Figure 5). Further, the gp41-reactivity of the anti-T88 polyclonal sera from these two rabbits was inhibited by three different epitope-scaffolds tested (T36, T161, and T163) but not by a “dead-epitope” version of the T36 epitope-scaffold (Figure 5), demonstrating specific reactivity to the helical structure of the 4E10 epitope stabilized on the scaffolds.

To assess the fine specificities of the anti-T88 polyclonal sera and mAb 4E10 across the helical epitope, we measured the binding of both sera and mAb to alanine-substituted 4E10 peptides using a multiplexed Luminex assay (Opalka et al., 2003). The results are displayed in Figure 6 as “relative avidity” in which the avidity for each ala mutant is divided by the avidity of mAb 4E10 for the wild-type peptide. A relative avidity significantly less than 1.0 indicates engagement of a particular side chain, as mutations to alanine should not detract from peptide helical propensity. Strikingly, the results indicated that both T88 sera strongly engaged most epitope side chains transplanted onto the T88 scaffold, as relative avidities for ala mutants at gp41 positions 672–675 (WFDI) and L679 were less than 0.3 ($p < 0.03$ in all cases except sera2 at I675 where relative avidity was less than 0.4 with $p = 0.02$). Two transplanted epitope side chains (T676 and W680) were engaged by one of the sera but not both; T676 relative avidity was 0.33 ± 0.28 for sera1 (engaged with relative avidity < 0.7 , $p = 0.02$) but 1.61 ± 0.33 for sera2, and W680 relative avidity was 0.49 ± 0.21 for sera2 (engaged with relative avidity < 0.8 , $p = 0.01$) but 0.74 ± 0.50 for sera1. Relative avidities for mAb 4E10 showed a similar overall pattern of side-chain engagement, except that mAb 4E10 did not engage I675 (relative avidity, 1.35 ± 0.18) and did strongly engage T676 (relative avidity, 0.08 ± 0.05). The data for mAb

4E10 agreed with previous competitive ELISA experiments (Brunel et al., 2006) except at positions 675 and 680 where Luminex indicated no mAb engagement but competitive ELISA (Brunel et al., 2006) indicated moderate engagement. As expected, neither of the two T88 sera nor mAb 4E10 had significantly altered avidity for ala mutations of gp41 residues N677 and W678 that are located on the opposite face of the helix from the WFDITxxLW epitope of 4E10 and were not transplanted onto the T88 scaffold.

Gp41-specific IgG was purified from the anti-T88 polyclonal sera and tested for fine specificity and neutralization. The fine specificity of the gp41-specific IgG was consistent with that of the sera in Figure 6. Neither the sera nor purified and concentrated anti-gp41 IgG reproducibly neutralized HIV-1 in an in vitro neutralization assay (not shown).

DISCUSSION

Here, we presented a new technique, computational design of epitope-scaffolds, to design immunogens that preserve the structure of a conserved epitope and expose that structure on a variety of different protein scaffolds with different immunologic backgrounds. We transplanted a conserved HIV epitope to multiple non-HIV proteins and succeeded to produce small, stable, soluble proteins with high affinity for the target monoclonal (K_D s < 1 nM). Indeed, several epitope-scaffolds bound mAb 4E10 up to 1000-fold more strongly than cognate peptide ($K_D \sim 10$ pM for epitope-scaffolds versus 10 nM for peptide). Crystal structures of multiple scaffolds demonstrated near perfect mimicry of the desired epitope backbone conformation ($rmsd \leq 1$ Å). We demonstrated the utility of epitope-scaffolds as serologic reagents to identify the presence or absence of antibodies targeting specific structural epitopes; this diagnostic utility conceptually extends to the use of epitope-scaffolds as “bait” for isolating such antibodies from libraries. Most importantly, we demonstrated that antibodies specific for the helical structure and the conserved side chains of the 4E10 epitope could be elicited by immunization with one such 4E10 epitope-scaffold. In contrast, immunization with peptide-KLH failed to elicit this desired specificity, and previous studies showed that several different constructs competent for 4E10 binding failed to elicit any detectable reactivity to the 4E10 linear sequence (Derby et al., 2006; Kim et al., 2007; Law et al., 2007). This example suggests the potential power of epitope-scaffolding; with the technique described here, many types of contiguous epitopes could be transplanted onto scaffolds for structural stabilization and immune presentation, and epitope-structure-specific immune responses might be further enhanced by glycan or PEG masking of the scaffold, by multimeric, oriented display of epitope-scaffolds on particles, by heterologous prime-boost immunizations, or combinations thereof. We also note that the epitope-scaffold concept is not limited to scaffolding of antibody epitopes, it could also prove useful to study, or design inhibitors for, peptide-protein and protein-protein interactions.

To our knowledge, the antibodies elicited by T88 are the first induced by vaccination to possess structural specificity highly similar to that of 4E10. This is an important advance for HIV vaccine design, because the helical specificity possessed by 4E10 and also the neutralizing sera in VC10028 (Sather et al.,

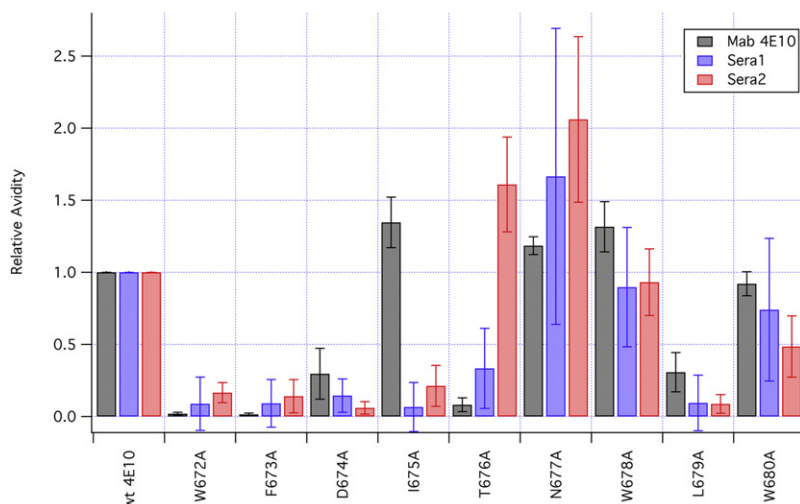


Figure 6. Luminex Analysis of bNAb 4E10 and Anti-T88 Rabbit Sera Binding to Ala-Scanned gp41 Peptides on Beads

Relative avidity for bNAb 4E10 (black) and two different anti-T88 rabbit sera (blue, PEI adjuvant; red, QS21 adjuvant) quantifies the avidity of each antibody/peptide or antisera/peptide pair relative to bNAb 4E10 binding to wild-type 4E10 peptide. Both anti-T88 antisera exhibit low relative avidity for mutants W672A, F673A, D674A, I675A, and L679A, which indicates that the antisera strongly engaged the 4E10 side chains at those positions on the helical epitope. Data were averaged from five experiments each run in duplicate; error bars represent mean \pm SD.

2009) is likely necessary for neutralization via the 4E10 epitope. The T88 antisera elicited by these first-generation designs did not neutralize HIV, however, indicating that helical specificity and the engagement of the conserved side chains of the 4E10 peptide epitope may not be sufficient. This result is consistent with recent studies demonstrating that specific hydrophobic residues on the tip of the 4E10 CDRH3 are required for maximum potency neutralization: alanine (Alam et al., 2009; Scherer et al., 2010; Xu et al., 2009) and aspartic acid (Scherer et al., 2010) substitutions at the tip do not significantly reduce gp41 or epitope-peptide binding, but they do reduce both lipid binding (Alam et al., 2009; Scherer et al., 2010; Xu et al., 2009) and the extraction of the epitope from the membrane (Xu et al., 2009), either mechanism potentially contributing to neutralization potency. As mentioned above, the tip of the 4E10 CDRH3 does not contact the peptide epitope used as the basis of the design of these first-generation epitope-scaffolds (Cardoso et al., 2005, 2007; Xu et al., 2009); further, no contacts with the CDRH3 tip are seen in Fv 4E10/epitope-scaffold complex structures as this was not a design criteria. Next-generation epitope-scaffolds incorporating higher order structural complementarity, such as viral membrane lipid structures, will be employed to improve on this approach.

In summary, we introduced a computational methodology that allows the faithful transplantation of conformational epitopes into distinct protein platforms and demonstrated that this leads to the appropriate stimulation of humoral responses to a conserved, but intrinsically poorly immunogenic viral epitope. Epitope-scaffolds therefore expand the universe of immunogens available for vaccine research. For the case of 4E10, computationally designed scaffolds can next be presented to the immune system in the context of lipid membrane surfaces, in combination with specific adjuvants to elicit antibodies with expanded recognition and neutralization properties.

EXPERIMENTAL PROCEDURES

Computational Design of Epitope-Scaffolds

The automated matching and design stages of the side-chain grafting protocol were implemented in the Rosetta (Das and Baker, 2008) modeling platform.

The matching stage exhaustively searched 13337 single chains from the PDB (Berman et al., 2000) for backbone similarity with the 4E10 epitope by computing rmsd between residues 671–680 or 672–680 in PDB ID:2FX7 (Cardoso et al., 2007) and all possible protein segments

using matched-width sliding windows in the query scaffolds. All hits with rmsd < 1 Å (or rmsd/length < 0.1) were retained if backbone clash with antibody was less than 100 score units. Epitope side chains were transferred to all-glycine versions of the remaining hits, and then interfacial side-chain torsions and the rigid-body orientation of antibody and epitope-scaffold were optimized by minimization (Gray et al., 2003). Highly conserved epitope side chains W672, F673, I675, L679, and W680 were transplanted to all scaffolds. At moderately variable epitope positions (671, 674, 676), the most energetically favorable of the common HIV side chains was generally transplanted (N, S, or G at 671; D, S, or N at 674; S or T at 676). Native scaffold side-chain rotamers outside the epitope were recovered, and residues near (heavy atom distance < 4 Å) the epitope or the antibody were designed, categorized as “intra” and “inter” positions, respectively. Inter residues were allowed to be ALA, GLY, SER, and THR, and intra positions were allowed to be all amino acids except CYS. Epitope-scaffolds were ranked by antibody binding energy and human-guided design was performed on the best to a) revert unnecessary or potentially destabilizing mutations; b) eliminate unpaired cysteines and undesired functional sites; c) trim extraneous domains; and d) optimize solubility. In two cases (T93 and T278), more advanced flexible backbone design was performed for domain trimming (T93) or fusion to maltose binding protein (MBP) for stabilization (T278); discussion of these methods is beyond the scope of this manuscript and will be reported elsewhere (B.E.C., Y.-E.A.B., D.J. Friend, K.E., H.X., E.B., T.B.-H., J.F.B.-J., L.S., R.K.S., and W.R.S., unpublished data).

Protein Expression, Purification, and Characterization

DNA segments encoding epitope-scaffold constructs were synthesized with optimized codon usage and RNA structure (Codon Devices, Genscript Corp.), subcloned into pET29 (EMD Biosciences), and transformed into BL-21 Star *E. coli* (Invitrogen). Single colonies were expanded from starter cultures in Luria Broth into ZYP-5052 autoinduction media (Studier, 2005) plus kanamycin (100 mg/ml), incubated for 4 hr at 37°C and then overnight at 18°C. Cultures were then pelleted and stored at -20°C . Pellets were resuspended in standard buffer (50 mM Tris, 500 mM NaCl, 10 mM imidazole, 0.5 mg/ml lysozyme), sonicated on ice, and clarified by centrifugation. Supernatants were tumbled with 10 ml of nickel-NTA resin (Superflow NTA, QIAGEN) for 30 min at 4°C. The resin was then rinsed twice with 10 mM imidazole, once with standard buffer plus 20 mM imidazole and eluted with standard buffer plus 250 mM imidazole. Eluates were concentrated by ultrafiltration (Amicon Ultra, Millipore) and filtered through 0.22 μm Ultrafree-MC spin columns (Millipore). Epitope-scaffolds were then purified by preparative size exclusion chromatography (SEC) on Superdex 75 16/60 columns (GE Healthcare) at room temperature in 25 mM PIPES (pH 7.0), 150 mM NaCl, 1 mM EDTA, and 0.02% w/w sodium azide (PNEA). Epitope-scaffold purity was confirmed by SDS-PAGE and analytical SEC; analytical SEC \pm target NAb (Superdex 75 or 200 10/30 columns, GE Healthcare) in PNEA was used to assay qualitative

binding, multimer state, monodispersity, and complex stoichiometries. Protein concentrations were determined with the BCA protein assay (Pierce); solution thermostabilities (T_m) were determined by circular dichroism (CD) spectroscopy with Jasco J-815 instrumentation as previously described (Xu et al., 2009).

In order to prepare endotoxin-free protein for immunization studies, bacterial pellets were alternately resuspended in detergent buffer (50 mM NaH_2PO_4 , 500 mM NaCl, 10 mM imidazole, 0.5 mg/ml lysozyme, 0.01 mg/ml DNase, 0.1% Triton X114) and loaded IMAC resin was alternately initially washed in 10 mM imidazole, 50 mM NaH_2PO_4 , 500 mM NaCl, 0.1% Triton X114.

Preparative SEC purification was carried out in sterile PBS on columns just previously cleaned with a bolus of 1 M NaOH. Endotoxin levels were assayed with the PyroGene Recombinant Factor C Endotoxin Detection System (Lonza). Protein preparations were further purified using the ProteoSpin Endotoxin Removal Maxi Kit (Norgen) if endotoxin levels exceeded 2EU/50 μg at a protein concentration of 1 mg/ml, the maximum level accepted for immunization.

Crystallization and Crystallography

Crystals of epitope-scaffolds and epitope-scaffold-Fv complexes were grown by vapor diffusion, under the conditions shown in Table S3. The complexes were purified as such by SEC prior to crystallization. Diffraction data were collected at -170°C on cryopreserved crystals, as detailed in Table 2, and processed with d*TREK (Pflugrath, 1999). Initial structure factor phases were determined by molecular replacement (search models in Table S3), using the program Phaser (McCoy et al., 2007) or MolRep (Vagin and Teplyakov, 1997), as implemented under CCP4i (Potterton et al., 2003). Successive rounds of modeling and positional and individual B factor refinement were carried out with Coot (Emsley and Cowtan, 2004) and Refmac5 (Murshudov et al., 1997). Five of the six structures were submitted to the TLSMD server (Painter and Merritt, 2006a, 2006b) where TLS groups were defined. Structure validation was carried out with Procheck (Laskowski et al., 1993), the MolProbity server (Davis et al., 2007), and the RCSB ADIT validation server. The structures were deposited in the PDB (Berman et al., 2000) with accession codes in Table S3. Data collection and structure refinement statistics are in Table 2.

Luminex Multiplex Assay

4E10 peptides with three lysines added to their C termini were amine-coupled to Bio-plex beads (Biorad, CA) (12 μg peptide/100 μl beads) as described by the manufacturer's protocol. Serially diluted sera (pre- and postimmunization) or mAb 4E10 were incubated with the bead cocktail for 1 hr at room temperature. After four washes, beads were incubated with anti-rabbit or human PE-conjugated secondary Ab for 1 hr at room temperature. A final wash step was performed prior to analysis on a Luminex 200 System (Invitrogen). Relative avidity was computed by subtracting peptide-matched, prebleed mean fluorescent intensity (MFI) from each sample MFI and then normalizing to the experiment-matched MFI for bNAb 4E10 binding to wild-type 4E10 peptide.

Peptide ELISA

Binding of rabbit sera or bNAb 4E10 to 4E10 peptide (NWFDTITNWLWYIRKKK) (Derby et al., 2006), alanine mutant 4E10 peptides, and epitope-scaffolds was assessed by ELISA as previously described (Derby et al., 2006).

Epitope-Scaffold Competitive ELISA

Rabbit sera (1:25) were incubated with epitope-scaffolds (100 $\mu\text{g}/\text{ml}$) for 1 hr, and then the mixture was added to ELISA plates coated with recombinant gp41 (HxB2) (0.5 $\mu\text{g}/\text{ml}$) (Meridian Life Science) for 90 min at 37°C . The binding of antibodies to gp41 was detected as above for the peptide ELISA.

Competing the Neutralizing Activity of HIV-1 + Sera by Epitope-Scaffolds

Epitope-scaffolds were tested for their ability to inhibit the neutralizing activity of plasma VC10028 as previously described for peptide inhibition (Sather et al., 2009).

Immunizations

Rabbits were immunized monthly at the Pocono Rabbit Farm and Laboratory Inc. (Canadensis, PA) with epitope-scaffolds mixed in PEI (Polysciences, Inc.)

or QS21 (Antigenics, Inc); 0.2 mg protein in 0.2 ml of PBS was administered into the two hind legs (0.2 ml per injection site). KLH peptide immunizations were performed by GenScript Corp (Piscataway, NJ); rabbits were immunized with 0.5 mg KLH peptide and complete Freund's adjuvant, and boosted at weeks 2, 5, and 8 with 0.5 mg KLH peptide and incomplete Freund's adjuvant. KLH peptide sera were tested from day 0 and week 10.

Statistical Analyses

We performed statistical analyses using a one-tailed Student's *t* test to obtain *p* values on the significance of relative avidity levels below specified thresholds.

ACCESSION NUMBERS

The crystal structures discussed in this paper were deposited in the PDB with following codes: 3LEF (T18), 3LH2 (T88-Fv), 3LHP (T93-Fv), 3LF6 (T117), 3LF9 (T161), and 3LG7 (T246).

SUPPLEMENTAL INFORMATION

Supplemental Information includes six figures and six tables and can be found with this article online at [doi:10.1016/j.str.2010.06.010](https://doi.org/10.1016/j.str.2010.06.010).

ACKNOWLEDGMENTS

We thank Della J. Friend for assistance with SPR and for comments on the manuscript. We thank Peter Kwong, Richard Wyatt, Gilad Ofek, and Javier Guenaga for discussions on scaffolding. QS21 adjuvant was provided by Antigenics, Inc. (Lexington, MA). This work was funded by a grant from the Bill and Melinda Gates Foundation CAVD to L.S., and B.E.C. was supported by a fellowship from Fundação para a Ciência e a Tecnologia (SFRH/BD/32958/2006). W.R.S., L.S., R.K.S., and D.B. conceived and supervised the study. Y.-E.A.B., and W.R.S. wrote the scaffold design software; B.E.C., Y.-E.A.B., C.C., and W.R.S. designed the scaffolds; E.B., C.Z., K.Y.B., T.B.-H., and J.F.B.-J. produced the proteins and performed SLS and SEC analysis; H.X., E.B., and O.K. performed SPR analysis; H.X. and E.B. performed CD melt analysis; M.A.H. crystallized many scaffolds and determined six crystal structures; B.E.C. and W.R.S. analyzed crystal structures; K.E. and Z.K. performed ELISA and Luminex analysis; D.N.S. performed neutralization competition assays; W.R.S. contributed statistical analysis; B.E.C., R.K.S., L.S. and W.R.S. wrote the paper; all authors commented on the manuscript.

Received: April 18, 2010

Revised: April 18, 2010

Accepted: June 1, 2010

Published: September 7, 2010

REFERENCES

- Alam, M., Morelli, M., Dennison, S.M., Liao, H.X., Zhang, R., Xia, S.M., and Rits-Volloch, S. (2009). Role of HIV membrane in neutralization by two broadly neutralizing antibodies. *Proc. Natl. Acad. Sci. USA* 106, 20234–20239.
- Berman, H.M., Westbrook, J., Feng, Z., Gilliland, G., Bhat, T.N., Weissig, H., Shindyalov, I.N., and Bourne, P.E. (2000). The Protein Data Bank. *Nucleic Acids Res.* 28, 235–242.
- Bianchi, E., Liang, X., Ingallinella, P., Finotto, M., Chastain, M.A., Fan, J., Fu, T.M., Song, H.C., Horton, M.S., Freed, D.C., et al. (2005). Universal influenza B vaccine based on the maturational cleavage site of the hemagglutinin precursor. *J. Virol.* 79, 7380–7388.
- Binley, J.M., Wrin, T., Korber, B., Zwick, M.B., Wang, M., Chappey, C., Stiegler, G., Kunert, R., Zolla-Pazner, S., Katinger, H., et al. (2004). Comprehensive cross-clade neutralization analysis of a panel of anti-human immunodeficiency virus type 1 monoclonal antibodies. *J. Virol.* 78, 13232–13252.
- Binley, J.M., Lybarger, E.A., Crooks, E.T., Seaman, M.S., Gray, E., Davis, K.L., Decker, J.M., Wycuff, D., Harris, L., Hawkins, N., et al. (2008). Profiling the specificity of neutralizing antibodies in a large panel of plasmas from patients

- chronically infected with human immunodeficiency virus type 1 subtypes B and C. *J. Virol.* **82**, 11651–11668.
- Brunel, F.M., Zwick, M.B., Cardoso, R.M., Nelson, J.D., Wilson, I.A., Burton, D.R., and Dawson, P.E. (2006). Structure-function analysis of the epitope for 4E10, a broadly neutralizing human immunodeficiency virus type 1 antibody. *J. Virol.* **80**, 1680–1687.
- Calarese, D.A., Scanlan, C.N., Zwick, M.B., Deechongkit, S., Mimura, Y., Kunert, R., Zhu, P., Wormald, M.R., Stanfield, R.L., Roux, K.H., et al. (2003). Antibody domain exchange is an immunological solution to carbohydrate cluster recognition. *Science* **300**, 2065–2071.
- Cardoso, R.M., Zwick, M.B., Stanfield, R.L., Kunert, R., Binley, J.M., Katinger, H., Burton, D.R., and Wilson, I.A. (2005). Broadly neutralizing anti-HIV antibody 4E10 recognizes a helical conformation of a highly conserved fusion-associated motif in gp41. *Immunity* **22**, 163–173.
- Cardoso, R.M., Brunel, F.M., Ferguson, S., Zwick, M., Burton, D.R., Dawson, P.E., and Wilson, I.A. (2007). Structural basis of enhanced binding of extended and helically constrained peptide epitopes of the broadly neutralizing HIV-1 antibody 4E10. *J. Mol. Biol.* **365**, 1533–1544.
- Das, R., and Baker, D. (2008). Macromolecular modeling with rosetta. *Annu. Rev. Biochem.* **77**, 363–382.
- Davis, I.W., Leaver-Fay, A., Chen, V.B., Block, J.N., Kapral, G.J., Wang, X., Murray, L.W., Arendall, W.B., 3rd, Snoeyink, J., Richardson, J.S., and Richardson, D.C. (2007). MolProbity: all-atom contacts and structure validation for proteins and nucleic acids. *Nucleic Acids Res.* **35**, W375–W383. doi: 10.1093/nar/gkm216.
- Derby, N.R., Kraft, Z., Kan, E., Crooks, E.T., Barnett, S.W., Srivastava, I.K., Binley, J.M., and Stamatatos, L. (2006). Antibody responses elicited in macaques immunized with human immunodeficiency virus type 1 (HIV-1) SF162-derived gp140 envelope immunogens: comparison with those elicited during homologous simian/human immunodeficiency virus SHIVSF162P4 and heterologous HIV-1 infection. *J. Virol.* **80**, 8745–8762.
- Dormitzer, P.R., Ulmer, J.B., and Rappuoli, R. (2008). Structure-based antigen design: a strategy for next generation vaccines. *Trends Biotechnol.* **26**, 659–667.
- Ekiert, D.C., Bhabha, G., Elsliger, M.A., Friesen, R.H., Jongeneelen, M., Throsby, M., Goudsmit, J., and Wilson, I.A. (2009). Antibody recognition of a highly conserved influenza virus epitope. *Science* **324**, 246–251.
- Emsley, P., and Cowtan, K. (2004). Coot: model-building tools for molecular graphics. *Acta Crystallogr. D Biol. Crystallogr.* **60**, 2126–2132.
- Frey, G., Peng, H., Rits-Volloch, S., Morelli, M., Cheng, Y., and Chen, B. (2008). A fusion-intermediate state of HIV-1 gp41 targeted by broadly neutralizing antibodies. *Proc. Natl. Acad. Sci. USA* **105**, 3739–3744.
- Gray, J.J., Moughon, S., Wang, C., Schueler-Furman, O., Kuhlman, B., Rohl, C.A., and Baker, D. (2003). Protein-protein docking with simultaneous optimization of rigid-body displacement and side-chain conformations. *J. Mol. Biol.* **331**, 281–299.
- Kashyap, A.K., Steel, J., Oner, A.F., Dillon, M.A., Swale, R.E., Wall, K.M., Perry, K.J., Faynboym, A., Ilhan, M., Horowitz, M., et al. (2008). Combinatorial antibody libraries from survivors of the Turkish H5N1 avian influenza outbreak reveal virus neutralization strategies. *Proc. Natl. Acad. Sci. USA* **105**, 5986–5991.
- Kim, M., Qiao, Z., Yu, J., Montefiori, D., and Reinherz, E.L. (2007). Immunogenicity of recombinant human immunodeficiency virus type 1-like particles expressing gp41 derivatives in a pre-fusion state. *Vaccine* **25**, 5102–5114.
- Klein, J.S., Gnanapragasam, P.N., Galimidi, R.P., Foglesong, C.P., West, A.P., Jr., and Bjorkman, P.J. (2009). Examination of the contributions of size and avidity to the neutralization mechanisms of the anti-HIV antibodies b12 and 4E10. *Proc. Natl. Acad. Sci. USA* **106**, 7385–7390.
- Kuhlman, B., Dantas, G., Ireton, G.C., Varani, G., Stoddard, B.L., and Baker, D. (2003). Design of a novel globular protein fold with atomic-level accuracy. *Science* **302**, 1364–1368.
- Laskowski, R.A., MacArthur, M.W., Moss, D.S., and Thornton, J.M. (1993). PROCHECK: a program to check the stereochemical quality of protein structures. *J. Appl. Crystallogr.* **26**, 283–291.
- Law, M., Cardoso, R.M., Wilson, I.A., and Burton, D.R. (2007). Antigenic and immunogenic study of membrane-proximal external region-grafted gp120 antigens by a DNA prime-protein boost immunization strategy. *J. Virol.* **81**, 4272–4285.
- Li, Y., Svehla, K., Louder, M.K., Wycuff, D., Phogat, S., Tang, M., Migueles, S.A., Wu, X., Phogat, A., Shaw, G.M., et al. (2009). Analysis of neutralization specificities in polyclonal sera derived from human immunodeficiency virus type 1-infected individuals. *J. Virol.* **83**, 1045–1059.
- McCoy, A.J., Grosse-Kunstleve, R.W., Adams, P.D., Winn, M.D., Storoni, L.C., and Read, R.J. (2007). Phaser crystallographic software. *J. Appl. Crystallogr.* **40**, 658–674.
- Murshudov, G.N., Vagin, A.A., and Dodson, E.J. (1997). Refinement of macromolecular structures by the maximum-likelihood method. *Acta Crystallogr. D Biol. Crystallogr.* **53**, 240–255.
- Ofek, G., Tang, M., Sambor, A., Katinger, H., Mascola, J.R., Wyatt, R., and Kwong, P.D. (2004). Structure and mechanistic analysis of the anti-human immunodeficiency virus type 1 antibody 2F5 in complex with its gp41 epitope. *J. Virol.* **78**, 10724–10737.
- Okuno, Y., Isegawa, Y., Sasao, F., and Ueda, S. (1993). A common neutralizing epitope conserved between the hemagglutinins of influenza A virus H1 and H2 strains. *J. Virol.* **67**, 2552–2558.
- Opalka, D., Lachman, C.E., MacMullen, S.A., Jansen, K.U., Smith, J.F., Chirmule, N., and Esser, M.T. (2003). Simultaneous quantitation of antibodies to neutralizing epitopes on virus-like particles for human papillomavirus types 6, 11, 16, and 18 by a multiplexed luminex assay. *Clin. Diagn. Lab. Immunol.* **10**, 108–115.
- Painter, J., and Merritt, E.A. (2006a). Optimal description of a protein structure in terms of multiple groups undergoing TLS motion. *Acta Crystallogr. D Biol. Crystallogr.* **62**, 439–450.
- Painter, J., and Merritt, E.A. (2006b). TLSMD web server for the generation of multi-group TLS models. *J. Appl. Crystallogr.* **39**, 109–111.
- Pflugrath, J.W. (1999). The finer things in X-ray diffraction data collection. *Acta Crystallogr. D Biol. Crystallogr.* **55**, 1718–1725.
- Phogat, S., Svehla, K., Tang, M., Spadaccini, A., Muller, J., Mascola, J., Berkower, I., and Wyatt, R. (2008). Analysis of the human immunodeficiency virus type 1 gp41 membrane proximal external region arrayed on hepatitis B surface antigen particles. *Virology* **373**, 72–84.
- Potterton, E., Briggs, P., Turkenburg, M., and Dodson, E. (2003). A graphical user interface to the CCP4 program suite. *Acta Crystallogr. D Biol. Crystallogr.* **59**, 1131–1137.
- Sather, D.N., Armann, J., Ching, L.K., Mavrantoni, A., Sellhorn, G., Caldwell, Z., Yu, X., Wood, B., Self, S., Kalams, S., and Stamatatos, L. (2009). Factors associated with the development of cross-reactive neutralizing antibodies during human immunodeficiency virus type 1 infection. *J. Virol.* **83**, 757–769.
- Scherer, E.M., Leaman, D.P., Zwick, M.B., McMichael, A.J., and Burton, D.R. (2010). Aromatic residues at the edge of the antibody combining site facilitate viral glycoprotein recognition through membrane interactions. *Proc. Natl. Acad. Sci. USA* **107**, 1529–1534.
- Stamatatos, L., Morris, L., Burton, D.R., and Mascola, J.R. (2009). Neutralizing antibodies generated during natural HIV-1 infection: good news for an HIV-1 vaccine? *Nat. Med.* **15**, 866–870.
- Stiegler, G., Kunert, R., Purtscher, M., Wolbank, S., Voglauer, R., Steindl, F., and Katinger, H. (2001). A potent cross-clade neutralizing human monoclonal antibody against a novel epitope on gp41 of human immunodeficiency virus type 1. *AIDS Res. Hum. Retroviruses* **17**, 1757–1765.
- Studier, F.W. (2005). Protein production by auto-induction in high density shaking cultures. *Protein Expr. Purif.* **41**, 207–234.
- Sui, J., Hwang, W.C., Perez, S., Wei, G., Aird, D., Chen, L.M., Santelli, E., Stec, B., Cadwell, G., Ali, M., et al. (2009). Structural and functional bases for broad-spectrum neutralization of avian and human influenza A viruses. *Nat. Struct. Mol. Biol.* **16**, 265–273.
- Sun, Z.Y., Oh, K.J., Kim, M., Yu, J., Brusica, V., Song, L., Qiao, Z., Wang, J.H., Wagner, G., and Reinherz, E.L. (2008). HIV-1 broadly neutralizing antibody

- extracts its epitope from a kinked gp41 ectodomain region on the viral membrane. *Immunity* 28, 52–63.
- Throsby, M., van den Brink, E., Jongeneelen, M., Poon, L.L., Alard, P., Cornelissen, L., Bakker, A., Cox, F., van Deventer, E., Guan, Y., et al. (2008). Heterosubtypic neutralizing monoclonal antibodies cross-protective against H5N1 and H1N1 recovered from human IgM+ memory B cells. *PLoS ONE* 3, e3942. doi: 10.1371/journal.pone.0003942.
- Vagin, A., and Teplyakov, A. (1997). MOLREP: an Automated Program for Molecular Replacement. *J. Appl. Crystallogr.* 30, 1022–1025.
- Watson, D.S., and Szoka, F.C., Jr. (2009). Role of lipid structure in the humoral immune response in mice to covalent lipid-peptides from the membrane proximal region of HIV-1 gp41. *Vaccine* 27, 4672–4683.
- Xu, H., Song, L., Kim, M., Holmes, M.A., Kraft, Z., Sellhorn, G., Reinherz, E.L., Stamatatos, L., and Strong, R.K. (2009). Interactions between lipids and human Anti-HIV antibody 4E10 can be reduced without ablating neutralizing activity. *J. Virol.* 84, 1076–1088.
- Zhou, T., Xu, L., Dey, B., Hessel, A.J., Van Ryk, D., Xiang, S.H., Yang, X., Zhang, M.Y., Zwick, M.B., Arthos, J., et al. (2007). Structural definition of a conserved neutralization epitope on HIV-1 gp120. *Nature* 445, 732–737.
- Zwick, M.B., Labrijn, A.F., Wang, M., Spencehauer, C., Saphire, E.O., Binley, J.M., Moore, J.P., Stiegler, G., Katinger, H., Burton, D.R., and Parren, P.W. (2001). Broadly neutralizing antibodies targeted to the membrane-proximal external region of human immunodeficiency virus type 1 glycoprotein gp41. *J. Virol.* 75, 10892–10905.